Heliyon 7 (2021) e07297

Contents lists available at ScienceDirect

Heliyon

journal homepage: www.cell.com/heliyon

Research article

Photocatalytic activity of $MnTiO_3$ perovskite nanodiscs for the removal of organic pollutants

Narasimharao Kitchamsetti [a], Pravin N. Didwal [b], Sameena R. Mulani [a], Madhuri S. Patil [a], Rupesh S. Devan [a,*]

[a] Department of Metallurgy Engineering and Materials Science, Indian Institute of Technology Indore, Simrol, Indore 453552, India
[b] Department of Materials Science and Engineering, Chonnam National University, 77, Yongbongro, Bukgu, Gwangju, 61186, South Korea

HIGHLIGHTS

- $MnTiO_3$ nanodiscs synthesized via hydrothermal method.
- The structure and composition of the perovskite $MnTiO_3$ nanodiscs were confirmed from XPS and TEM analysis.
- The optimal photocatalytic degradation of 89.7, 80.4, 79.4, and 79.4 % was observed after 180 min of irradiation for MB, RhB, MO, and CR, respectively.

ARTICLE INFO

Keywords:
$MnTiO_3$ perovskite
Organic pollutant
Photocatalyst
Dye degradation
TEM

ABSTRACT

MTO nanodiscs synthesized using the hydrothermal approach were explored for the photocatalytic removal of methylene blue (MB), rhodamine B (RhB), congo red (CR), and methyl orange (MO). The disc-like structures of ~16 nm thick and ~291 nm average diameter of stoichiometric MTO were rhombohedral in nature. The MTO nanodiscs delivered stable and recyclable photocatalytic activity under Xe lamp irradiation. The kinetic studies showed the 89.7, 80.4, 79.4, and 79.4 % degradation of MB, RhB, MO, and CR at the rate constants of 0.011(±0.001), 0.006(±0.001), 0.007(±0.0007), and 0.009 (±0.0001) min^{-1}, respectively, after the 180 min of irradiation. The substantial function of photogenerated holes and hydroxide radicals pertaining to the dye removal phenomena is confirmed by radical scavenger trapping studies. Overall, the present studies provide a way to develop pristine and heterostructure perovskite for photocatalysts degradation of various organic wastes.

1. Introduction

Nowadays, the raised industrialization frequently releases hazardous contaminants in the environment, especially organic pollutants in water and soil, which precedes detrimental effects on groundwater quality [1]. This contamination disturbs aquatic life, earth, and humans living directly or indirectly, which is a threat to a viable civilization [2]. Pharmaceutical garbage and organic wastes are mostly non-eco-friendly, and their removal from anaerobic environments gives rise to harmful ingredients in the atmosphere [3]. Chemical methods such as Fenton's reagent, ozonation, advanced oxidation processes, and anaerobic treatment, etc., and the physical processes such as adsorption, reverse osmosis, flocculation, and sedimentation, etc. have been explored to control pharmaceutical contaminants via degradation of organic dyes [4]. But, in recent times, photocatalysis has gained considerable attention as an environmentally friendly process where no further energy in the kind of heat is expected during the degradation processes. The most cost-effective photocatalyst is expected to be non-poisonous, reusable, and highly durable. Therefore, various metal oxides and sulfides of Ni, Ti, Zn, W, Cu, and Mo are explored for photocatalytic dye-degradation [5, 6, 7, 8]. However, oxidative degradation observed from metal oxides, without any substantial alterations in their properties, on exposure to the visible light has the potentials to serve in real-time applications, hence attracting the scientific community [9]. So far, TiO_2, ZnO, CuO, MnO_2, NiO, and Co_3O_4 are extensively studied to remove the synthetic pigments from the water bodies [5, 6]. TiO_2 remains the highly explored photocatalysts for removing synthetic dyes due to its chemical limpness, photocatalytic permanence, and eco-friendly nature [10]. However, a wide bandgap of 3.2 eV hampers the TiO_2 photocatalytic activities in the visible region. Therefore,

* Corresponding author.
E-mail address: rupesh@iiti.ac.in (R.S. Devan).

https://doi.org/10.1016/j.heliyon.2021.e07297
Received 1 April 2021; Received in revised form 7 May 2021; Accepted 9 June 2021
2405-8440/© 2021 Published by Elsevier Ltd. This is an open access article under the CC BY-NC-ND license (http://creativecommons.org/licenses/by-nc-nd/4.0/).

numerous tactics like doping and coupling with additional semiconducting materials were employed to boost the photocatalytic activity by controlling the bandgap of TiO_2 in the visible range [11, 12, 13]. On the other hand, the oxides of Mn deliver the narrow bandgap of 1–2 eV has the potentials to deliver promising photocatalytic activities in the visible region [14, 15]. The promising catalytic properties combined through acid resistance and natural profusion have denoted MnO_2 as a captivating contender in removing the organic dye.

The conformation of such narrow and wide bandgap oxide materials in the perovskite form shall enhance the photocatalytic activities. Moreover, perovskite oxides are contemplated to be an exhilarating group of visible-light photocatalytic materials in current times [16]. Perovskite oxides delivered excellent structural stability and flexibility to accommodate a wide range of cations with different oxidation states, which guided them for excellent catalytic activity and consequently for applications in photocatalysis [17, 18, 19, 20, 21]. Various research groups have explored the photocatalytic dye degradation activities of the perovskite materials such as $ZnTiO_3$, $SrTiO_3$, $BaTiO_3$, $NiTiO_3$, $CoTiO_3$, and $MnTiO_3$, respectively [20, 22, 23, 24, 25, 26]. Ali et al. [26] observed photocatalytic degradation of methyl orange (MO) using the cobalt titanate nanoparticles obtained from the polymerization method, but 50 % of methyl orange dye was removed after 80 min irradiation of UV light. $SrTiO_3$ removed 95 % of methylene blue (MB) dye after irradiating 360 min under visible light [23]. Likewise, the microwave-assisted $BaTiO_3$ nanospheres were found comparatively effective and quicker in the degradation of MB under UV light irradiation [24]. The longer time taken by these perovskites for degradation of organic dyes directed the scientific community to hunt for new materials with larger surface area and improved photocatalytic activities. $MnTiO_3$, a wide bandgap (i.e., 1.5–3.2 eV) perovskite [27], has recently attracted the attention for applications in magnetic recorder, solar cells, gas sensor, and dielectric ceramics, etc. due to the high carrier mobility, enormous absorption coefficient, exceptional photo-physical/chemical properties. Furthermore, the strong absorption in the visible region has governed the MTO as competent material for photocatalytic removal of organic dyes. He et al. [27] have reported the usefulness of MTO for photodegradation of MO under sunlight irradiation, but lower bandgap (i.e., 1.46 eV) of MTO nanoparticles restricted the absorption of visible light and inhibited the overall degradation performance. Recently, Suhila et al. [20] reported photodegradation of MB dye using the sol-gel synthesized MTO powders, but the total degradation was restricted to 70 % after 240 min irradiation. Nevertheless, the excellent physicochemical properties, together with the good agreement of Mn and Ti elements, navigate the MTO to explore the degradation activity of the various organic dyes. Consequently, various nanostructure morphologies of MTO need to be explored thoroughly to understand the effect of larger surface area, the stoichiometry of Mn and Ti, and O deficiency, etc.

Overall, the literature reports the independent studies on the utilization of MTO for the photocatalytic degradation of either MB or MO. Moreover, our recent studies revealed that the larger surface area enhances the photocatalytic decomposition of organic dyes [28]. Here, we report the comparative study on the photocatalytic removal of MB, RhB, MO, and CR dyes in the presence of MTO nanodiscs providing a larger surface area. The structural, chemical, morphological, and photocatalytic studies illustrate the competency of MTO nanodiscs for MB dye degradation under light illumination. The MTO nanodiscs might have provided abundant trapping sites for electrons, which influenced the electron-hole pair recombination and further assisted in enhancing photocatalytic dye removal activities.

2. Experimental section

The analytical grade reagents procured from Sigma Aldrich were used as collected to synthesize MTO nanodiscs using the hydrothermal method. Typically, 1.25 mmol of Tetrabutyl orthotitanate ($Ti(C_4H_9O)_4$, 98 %) was added to 16 ml of 1,2-Ethanediol ($C_2H_6O_2$, 99 %) under continuous stirring at room temperature to prepare a homogeneous solution. Simultaneously, 1.25 mmol of manganese chloride tetrahydrate ($MnCl_2.4H_2O$, 98 %) was dissolved into 4 ml of 1,2-diaminoethane ($C_2H_8N_2$, 99 %). Both these solutions were mixed for 30 min under constant stirring, and subsequently, 5 ml of deionized water was added dropwise and continued stirring. Later, the solution was moved to a Teflon-lined stainless-steel autoclave and reacted at 180 °C for 24 h, which was allowed to cool down at room temperature in the ambient atmosphere. The hydrothermally reacted product was collected by centrifugation after rinsing through deionized water and alcohol numerous times to discard additional impurities and solvent. Further, the MTO powder with pale-yellow color was achieved after drying at 90 °C for 8 h and characterized to analyze the physicochemical properties. The crystal structure of the MTO perovskite was verified using X-ray diffraction (D2-Phaser Bruker, Cu-Kα, λ = 1.5406 Å). The field emission scanning electron microscope (FESEM, JEOL JSM-6500F) equipped with energy-dispersive X-ray spectroscopy (EDS, Oxford Instrument INCA, X-sight 7557) was used to investigate the surface morphology of MTO and the presence of elements, respectively. X-ray photoelectron spectrometer (XPS, Thermo Scientific Inc. K-alpha) with microfocus monochromated Al Kα X-rays was used to investigate the surface chemistry and electronic nature of MTO nanodiscs. The optical behavior of MTO nanodiscs was studied using a UV-Visible spectrophotometer (Shimadzu UV-2600). The photocatalytic activity of MTO nanodiscs was analyzed for various organic dyes under Xe lamp (300 W) irradiation. The optimized amount of 25 mg MTO catalyst was added into 10 ppm aqueous dye solutions maintained at pH of 6.8 under continuous stirring for 1 h in the darkroom at ambient atmosphere to obtain an adsorption-desorption equilibrium between the dye pollutant and photocatalyst before the light illumination. It was further irradiated under Xe lamp at different time intervals and centrifuged to extract the catalyst from the dye solution. The centrifuged solution was further subjected for UV-Vis absorption studies. The concentration (C_t) at a reaction time of 't' and the initial concentration (C_o) of the dye pollutants were examined instantly from UV-Vis spectra. The degradation rate of different dye solutions was estimated from the Eq. (1),

$$\text{Dye degradation efficiency } (\%) = \frac{C_o - C_t}{C_o} \times 100 \quad (1)$$

3. Results and discussion

FESEM image in Figure 1(a) reveals the morphology of MTO nanodiscs. The optimized reaction mixture of $MnCl_2$, $Ti(C_4H_9O)_4$, and $C_2H_6O_2$ offered a disc-like morphology of MTO. Even though the diameter of ~16 (±3) nm thick nanodiscs varied between 180 to 440 nm, most nanodiscs were of 291 (±5) nm average diameter. Each nanodisc was intact and separated from the other with clearly visible boundaries. The high magnification FESEM image in the inset of Figure 1(a) illustrates the rough surface morphology of the MTO, which provided the BET surface area of 64.6 m^2/g and the pore volume of 0.11 cm^3/g. The EDS image of MTO nanodiscs confirms the presence of Ti, Mn, and O elements, without detecting any extra elements except C. The insignificant existence of C might have observed from the carbon tape utilized during the analysis (Figure 1(b)). Further, the crystal structure MTO nanodiscs was studied utilizing XRD. The resulting XRD peaks (Figure 1(c)) located at 2θ of 23.5°, 32°, 34.8°, 39.8°, 48.1°, 52.2°, 55.1°, 60.8°, 62.5°, and 68.7° corresponds to (012), (104), (110), (113), (024), (116), (018), (214), and (300), respectively, are assigned to the rhombohedral crystal structure MTO (JCPDS card no. 12-0435). Furthermore, no distinctive peaks specifying the development of TiO_2, MnO_2, or additional impurity phases were observed, corroborate the synthesis of single-phase MTO nanodiscs. Further, the crystal structure of the MTO was confirmed from TEM analysis. The HRTEM image (Figure 2(a)) confirms that the MTO nanodiscs were well crystallized with an interplanar spacing of 0.352 nm comprised of (012) rhombohedral lattice plane [29]. Moreover, the SAED

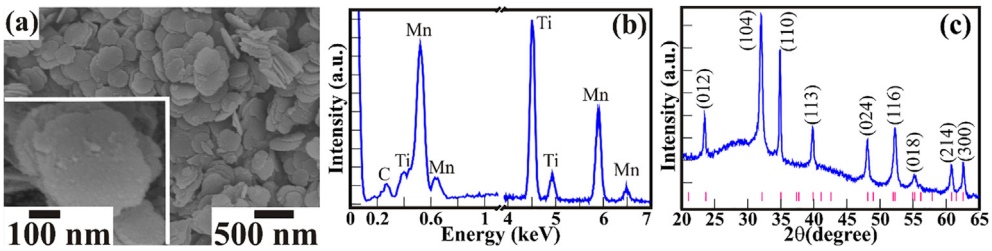

Figure 1. (a) FESEM image, (b) EDS, and (c) XRD pattern of MTO nanodiscs.

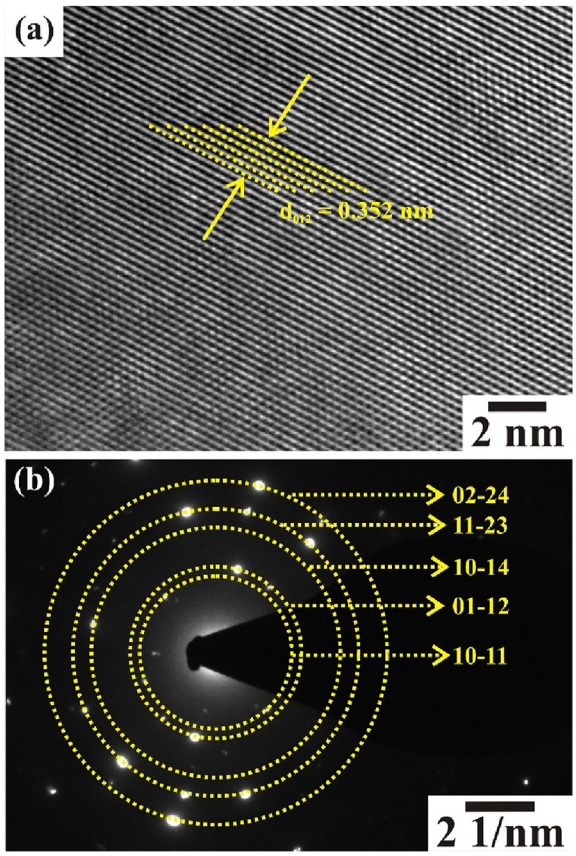

Figure 2. (a) HRTEM image (b) SAED pattern collected from the MTO nanodiscs.

pattern of the MTO nanodiscs represents randomly aligned numerous diffraction spots (Figure 2(b)). The careful observation of these numerous bright diffraction spots produces concentric diffraction rings (yellow in color) correspond to the rhombohedral crystal structure of MTO nanodiscs. These observations are akin to that of XRD, EDS, and FESEM analysis.

Moreover, the chemical properties and electronic structure of MTO nanodiscs were analyzed employing XPS. Figure 3 illustrates the XPS spectra of Mn(2p), Ti(2p), and O(1s) core levels of MTO nanodiscs. The XPS spectrum of Mn(2p) was fitted via the Voigt function to accurately define the double peak features of Mn ($2p_{3/2}$) and Mn ($2p_{1/2}$) core levels [30]. The deconvoluted XPS of Mn(2p) (Figure 3(a)) displays 4 peaks positioned at binding energy (B.E.) of 641.5 (≡ A), 645.6 (≡ A′), 653.2(≡ B), and 657.1 eV (≡ B′). The peaks situated at a B.E. of 641.5 (≡ A) and 653.2 (≡ B) eV have been allocated to the core levels of Mn(2p), and their associated peaks at a binding energy of 645.6 (≡ A′) and 657.1 (≡ B′) are relevant shake-up satellite peaks. The peak splitting of 11.7 eV between the Mn ($2p_{3/2}$) and Mn ($2p_{1/2}$) core levels represents the formation of Mn^{2+}. Similarly, the deconvolution of XPS spectrum of the Ti(2p) core levels demonstrate the three distinct peaks at the B.E. of 458.3 (≡ C), 460.2 (≡ C′), and 463.9 (≡ D) eV for the $Ti^{4+}(2p_{3/2})$, $Ti^{3+}(2p_{3/2})$ and $Ti^{4+}(2p_{1/2})$ core levels, respectively. The greater intensity of $Ti^{4+}(2p_{3/2})$ and $Ti^{4+}(2p_{1/2})$ peaks represents the major existence of Ti^{4+} cation. However, the less intense peak of $Ti^{3+}(2p_{3/2})$ core levels proves the minor presence of Ti^{3+} cations. The peak separation of 5.6 eV between the Ti($2p_{3/2}$) and Ti($2p_{1/2}$) core levels suggest Ti^{4+} cations [18, 19, 31]. The compound peak characteristic for O(1s) XPS spectrum deconvoluted using Voigt fitting function (Figure 3(c)) revealed 2 peaks at a binding energy of 529.5 and 531.1 eV. The high-intensity peak at 529.5 eV resembles the O(1s) core level of the O^{2-} anions in the MTO nanodiscs. The less intensity peak at 531.1 eV is assigned to the surface contamination, in the form of carbon or hydroxides, etc. [28, 32]. In general, the XPS study validates the formation of stoichiometric MTO nanodiscs.

The UV-Vis spectroscopy was employed to inspect the optical behavior of the MTO nanodiscs. The optical diffusive reflectance spectra (DRS) of the MTO nanodiscs was evaluated at room temperature. Figure 4 presents the typical reflectance spectra of MTO nanodiscs, which was further analyzed to evaluate energy bandgap using the Kubelka-Munk function in Eq. (2),

$$(F(R))^{0.5} = \frac{(1-R)^2}{2R} \times h\nu \qquad (2)$$

Where, R is the absolute reflectance of the MTO, and hν is incident photon energy. The bandgap is evaluated from the plots of $(F(R)\ h\nu)^{1/2}$ versus hν, believing that the absorption coefficient (α) is directly proportional to the Kubelka-Munk function (F(R)). The bandgap of 2.78 eV was approximated from the (hυ) vs. $(F(R)\ h\nu)^{1/2}$ plot for MTO nanodiscs. The reduced thickness (i.e., dimensions) of the MTO nanodiscs might be the reason for the increase in the bandgap than the bulk MTO [27]. The photocatalytic degradation studies of MTO nanodiscs were performed on MB, RhB, MO, and CR dyes under continuous Xenon lamp illumination at ambient atmosphere. The irradiated solutions were collected at different time intervals, and their consecutive UV-Vis spectra are shown in Figure 5. The intensity of the major absorption peak of MB (i.e., 664 nm), RhB (i.e., 554 nm), MO (i.e., 463 nm), and CR (i.e., 498 nm) continued reducing with an increase in irradiation time, which confirm the removal of dye pollutants under xenon lamp irradiation in the presence of MTO photocatalysts. The dye removal has improved with increased irradiation time and reached saturation after attending the highest dye removal in 180 min of illumination. However, for a better understanding of the photocatalytic degradation activity of MTO nanodiscs, the MB was irradiated in the absence of photocatalyst for the identical time period (i.e., 180 min) [33]. An insignificant amount of dye removal detected in the absence of MTO nanodiscs (Figure 6) confirmed the influence of MTO nanodiscs in the photocatalytic degradation of dye pollutants. The excellent absorption of pollutants and the photosensitizing effect of the MTO nanodiscs might have helped consume a significant amount of visible light to enhance the photocatalytic mechanism [34].

The reaction kinetics of photocatalytic dye removal was comprehended from the Langmuir-Hinshelwood model (Eq. (3)) [35], which is simplified to the pseudo-first-order equation for a lower concentration of catalysts (Eq. (4)),

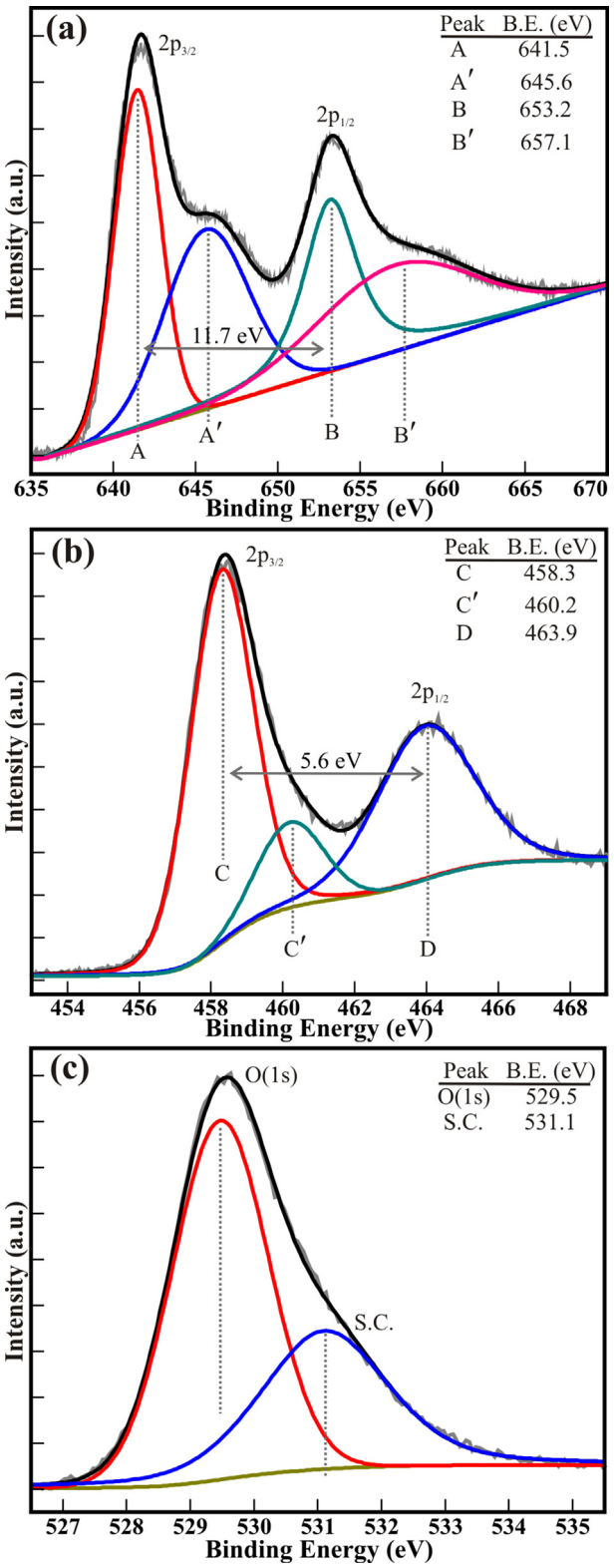

Figure 3. High resolution XPS spectra of the (a) Mn (2p), (b) Ti (2p), and (c) O (1s) core levels of the MTO nanodiscs.

$$r = \frac{-dc}{dt} = \frac{Kkc}{(1 + CK)} \tag{3}$$

$$r = \frac{-Dc}{dt} = k_{obs}C, \quad \text{i.e.,} \quad -\ln\frac{C_t}{C_o} = k_{obs}t \tag{4}$$

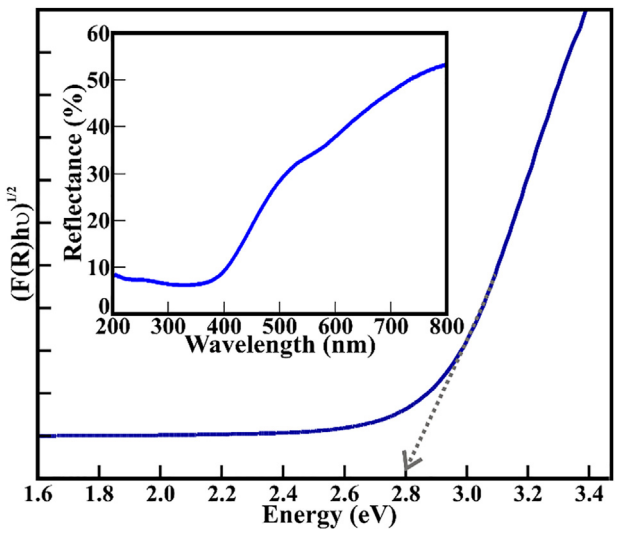

Figure 4. UV-Vis DRS spectra and bandgap analysis of MTO nanodiscs.

Where, r is the reaction rate in mol/L.min, C is the equilibrium concentration of the constituent in mol/L, t is the photocatalytic activity time in min., K is the Langmuir constant in L/mol, k is the reaction rate constant in L/min, C_t and C_o are the dye pollutant concentrations in mol/L at various time intervals (t) and t = 0, and k_{obs} is the pseudo-first-order rate constant in L/min.

The photocatalytic degradation activities are illustrated using the pseudo-first-order kinetic model. Figure 7(a and b) signifies the plot of C_t/C_0 and –ln (C_t/C_0) with respect to the irradiation time (t) for the MB, RhB, CR, and MO dye removal estimated from Figure 5. The photocatalytic dye pollutant removal mechanism is tailored well with the pseudo-first-order kinetics model. The rate constant of 0.011(±0.001), 0.0064(±0.001), 0.009(±0.0001), and 0.007(±0.001) min^{-1}, and correlation coefficient (R^2) of 0.94, 0.89, 0.99, and 0.95 were observed for MB, RhB, MO, and CR dye, respectively. The higher rate constant represents the improved response of MTO nanodiscs for photocatalytic decomposition of MB than the RhB, MO, and CR dyes. Figure 7(c) reveals the statistical histogram of irradiation time-dependent dye degradation efficiency estimated from Figure 5. The 89.7, 80.4, 79.4, and 79.4 % photocatalytic decomposition was detected for MB, RhB, MO, and CR dyes, respectively, after 180 min irradiation. This reveals that MTO nanodiscs show superior photocatalytic activity for MB.

Being the better photocatalytic reaction mechanism of MTO towards MB, the radical scavenger catching studies were carried out for photocatalytic decomposition of MB in the presence of various scavengers. Figure 8(a) shows the photocatalytic decomposition of MB in the existence of distinct scavengers such as methanol (MeOH), isopropanol (IPA), and ammonium oxalate (AO) to confirm the influence of superoxide radicals ($*O_2^-$), hydroxyl radicals (OH*), and photogenerated holes (h^+), respectively [36]. The severely reduced photodegradation of MB (i.e., 19.8 %) in the presence of AO confirms the significant role of photogenerated holes in MB decomposition. However, the moderate reduction in the photodegradation (i.e., 35 %) in the presence of IPA confirms the partial involvement of hydroxyl radicals (OH*). Thus, the hydroxyl radicals (OH*) and photogenerated holes (h^+) dominated the photodegradation of the MB. Further, the reusability of MTO nanodiscs was examined for three repeated cycles of MB degradation (Figure 8(b)). The negligible loss of ~2 % (i.e., from 89.7 % to 87 %) observed in the photocatalytic degradation activity for MB dye might be attributed to the catalyst loss throughout the recovery processes such as washing, centrifugation, and desiccating, etc. Moreover, the stability of MTO nanodiscs photocatalysis was confirmed from FTIR. The FTIR spectra of the MTO nanodiscs before and after photocatalytic studies (Figure 9) were

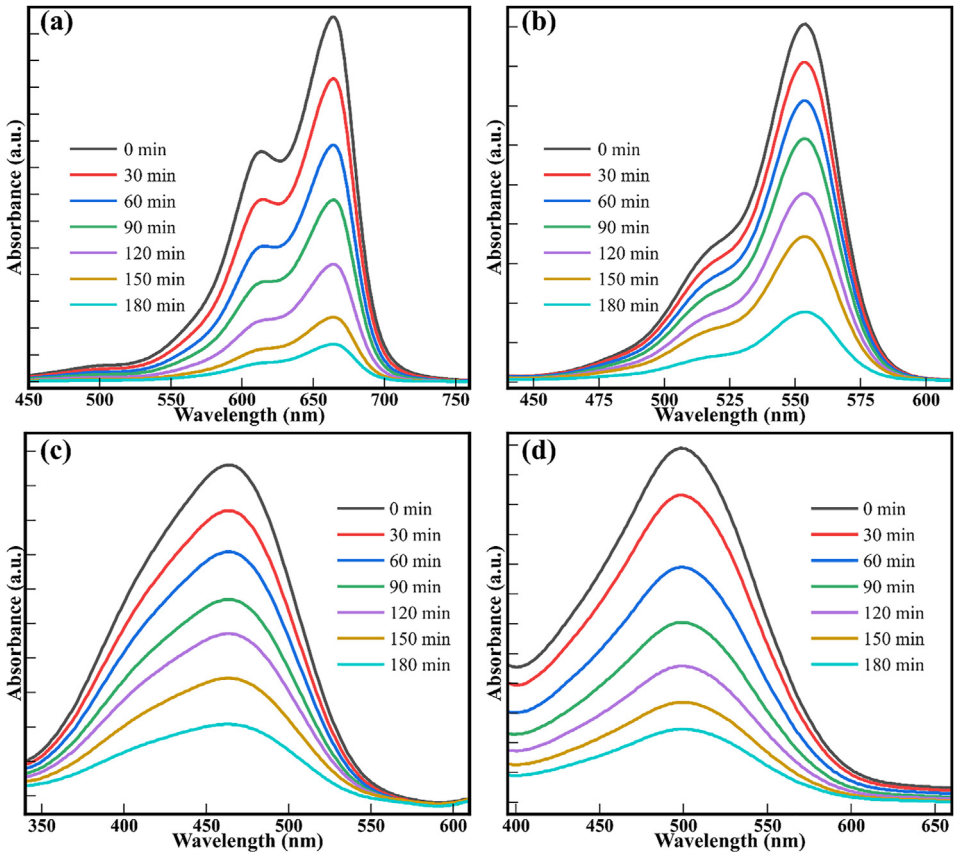

Figure 5. Time-dependent UV-Vis absorption spectra of (a) MB, (b) RhB, (c) MO, and (d) CR dye pollutants collected at regular intervals for 180 min irradiation in the presence of 25 mg MTO catalyst.

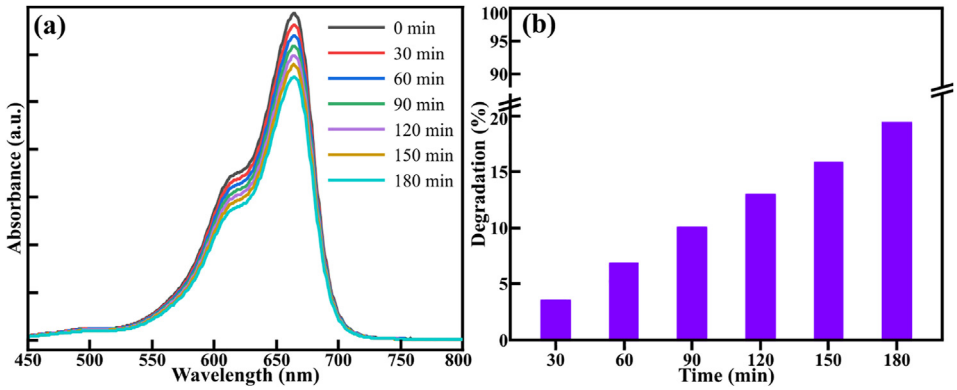

Figure 6. (a) UV-Visible absorption spectra and (b) histogram of degradation percentage of MB dye solution collected at regular intervals for photocatalytic irradiation of 180 min without photocatalyst.

identical to each other, illustrate the excellent photocatalytic stability of the MTO nanodiscs.

Figure 10 illustrates a pictorial representation of the photocatalytic degradation behavior of MTO nanodiscs. The electron (e^-) – hole (h^+) pair photogenerated after xenon light irradiation control the photocatalytic activity of MTO nanodiscs. Therefore, photocatalytic degradation depends on (i) trapping and recombination of holes and electrons and (ii) recombination of the captured electron (e^-) – hole (h^+) pair. The increased e^- – h^+ recombination time and the larger interface of the electron transfer rate boost the photocatalytic decomposition. In the current work, the photocatalytic decomposition mechanism of dye pollutant is described as follows:

$$MTO + h\upsilon \rightarrow MTO\ (e^- + h^+) \quad (5)$$

$$MTO\ (e^-) + O_2 \rightarrow MTO\ (*O_2^-) \quad (6)$$

$$Dye + *O_2^- \rightarrow Dye_{ox}\ (intermediates) \rightarrow CO_2 + H_2O \quad (7)$$

$$MTO\ (h^+) + H_2O \rightarrow MTO\ (OH^*) + H^+ \quad (8)$$

$$Dye + OH^* \rightarrow Dye_{ox}\ (intermediates) \rightarrow CO_2 + H_2O \quad (9)$$

Under visible light illumination with sufficient energy of photon greater than or equal to the bandgap of MTO nanodiscs, electrons (e^-) are excited from the valence band (V.B.) to the conduction band (C.B), leaving holes in the V.B., which are created and then recombine on the

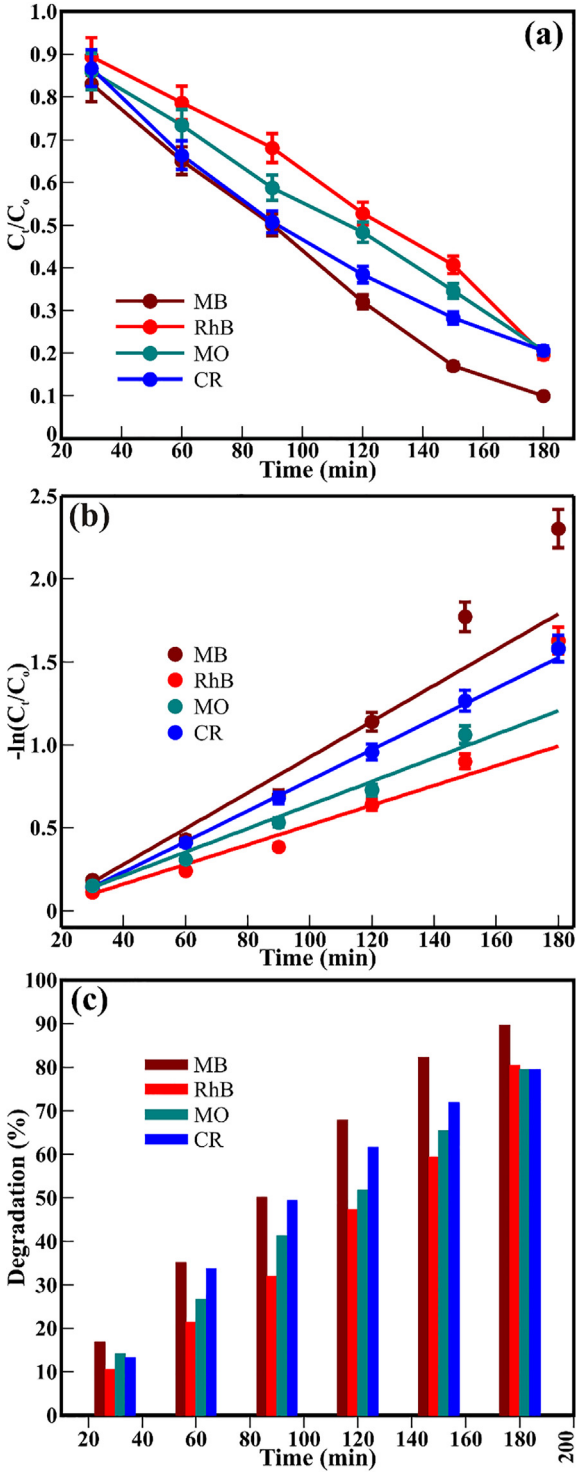

Figure 7. (a) Kinetic plots, (b) subsequent pseudo-first-order kinetic curves, and (c) histogram of dye removal percentage estimated for photocatalytic reduction of MB, RhB, MO, and CR dyes in the presence of 25 mg MTO nanodiscs.

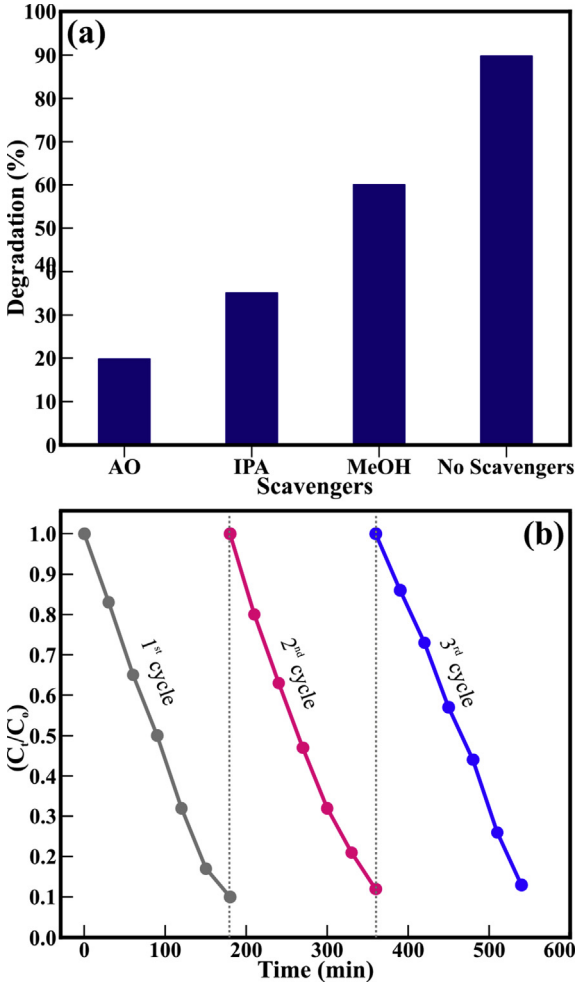

Figure 8. (a) Effect of different scavengers and (b) cyclic stability performance of MTO nanodiscs in the photocatalytic removal of MB.

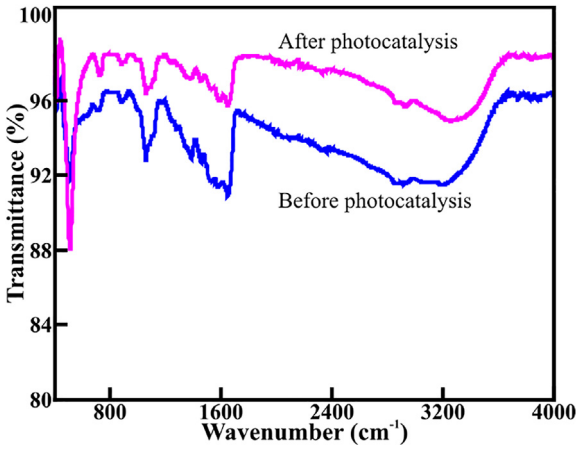

Figure 9. FTIR spectra, obtained from the MTO nanodiscs before and after three repeated photocatalytic degradation cycles of MB dye solution.

MTO surface (Eq. (5)). MTO nanodiscs capture the electrons, which arrests electron (e^-) - hole (h^+) recombination and improve the $*O_2^-$ radicals for degradation of the dyes (Eqs. (6), and (7)) [37]. In most cases, holes may easily react with H_2O to generate *OH radicals (Eq. (8)) [38]. It is well-known that *OH radicals are robust oxidizing agents efficient for degrading most dye contaminants. The dyes may be oxidized by *OH radicals (Eq. (9)) and then be reduced to small organic pieces, and these organic pieces can ultimately be mineralized into CO_2 and H_2O. Therefore, the larger surface area and disc-like morphology of MTO have a significant impact on the eco-friendly and economic photocatalytic mechanism for transforming various organic chemicals/pollutants.

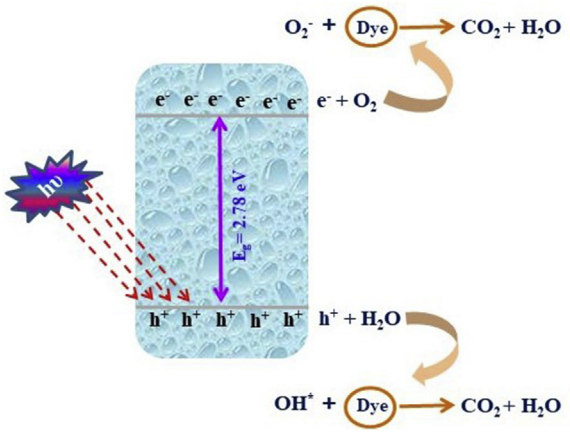

Figure 10. Schematic representation of the photocatalytic mechanism of MTO nanodiscs in dye pollutants removal.

4. Conclusion

In conclusion, we have successfully synthesized MTO nanodiscs via the hydrothermal method. The MTO nanodiscs of thickness ~16 nm and a diameter of ~291 nm were of the rhombohedral crystalline phase. The stoichiometric MTO nanodiscs delivered the bandgap of 2.78 eV and unveiled the exceptional photocatalytic activity to decompose organic pollutants. The optimal photocatalytic reduction of 89.7, 80.4, 79.4, and 79.4 % was observed after 180 min for MB, RhB, MO, and CR, respectively, at the 0.011(±0.001), 0.0064(±0.001), 0.009(±0.0001), and 0.007(±0.001) min^{-1}, rate constants. The stability and recyclability without substantial loss in photocatalytic activity conclude the reliable, economic, and eco-friendly nature of MTO nanodiscs.

Declarations

Author contribution statement

Narasimharao Kitchamsetti: Performed the experiments; Analyzed and interpreted the data; Wrote the paper.

Pravin N. Didwal, Sameena R. Mulani, Madhuri S. Patil: Analyzed and interpreted the data.

Rupesh S. Devan: Conceived and designed the experiments; Analyzed and interpreted the data; Contributed reagents, materials, analysis tools or data; Wrote the paper.

Funding statement

This work was supported by UGC-DAE CSR Indore (Grant No.: CSR-IC-BL65/CRS-182/2017-18/189, and SERB-DST India (Grant No.: TAR/2019/000106). Narasimharao Kitchamsetti was supported by IIT Indore (Institute Fellowship) for doctoral research work.

Data availability statement

Data will be made available on request.

Declaration of interests statement

The authors declare no conflict of interest.

Additional information

No additional information is available for this paper.

References

[1] J. Porras, C. Bedoya, J.S. Agredo, A. Santamaria, J.J. Fernandez, R.A. Torres-Palma, Role of humic substances in the degradation pathways and residual antibacterial activity during the photodecomposition of the antibiotic ciprofloxacin in water, Water Res. 94 (2016) 1–9.

[2] L. Qin, H.Z. Chen, J. Lei, Y.Q. Wang, T.Q. Ye, H.G. Zheng, Photodegradation of some organic dyes over two metal-organic frameworks with especially high efficiency for safranine T, cryst, Growth Des. 17 (2017) 1293–1298.

[3] S. Kumar, V. Sharma, K. Bhattacharyya, V. Krishnan, Synergetic effect of MoS_2-RGO doping to enhance the photocatalytic performance of ZnO nanoparticles, New J. Chem. 40 (2016) 5185–5197.

[4] Y.M. Slokar, A.M. Le Marechal, Methods of decoloration of textile wastewaters, Dyes Pigments 37 (1998) 335–356.

[5] J.H. Kou, J. Gao, Z.S. Li, Z.G. Zou, Research on photocatalytic degradation properties of organics with different new photocatalysts, Curr. Org. Chem. 14 (2010) 728–744.

[6] L. Gnanasekaran, R. Hemamalini, R. Saravanan, K. Ravichandran, F. Gracia, S. Agarwal, V.K. Gupta, Synthesis and characterization of metal oxides (CeO_2, CuO, NiO, Mn_3O_4, SnO_2 and ZnO) nanoparticles as photocatalysts for degradation of textile dyes, J. Photochem. Photobiol., B 173 (2017) 43–49.

[7] M.S.S. Danish, L.L. Estrella, I.M.A. Alemaida, A. Lisin, N. Moiseev, M. Ahmadi, M. Nazari, M. Wali, H. Zaheb, T. Senjyu, Photocatalytic applications of metal oxides for sustainable environmental remediation, Metals 11 (2021) 80.

[8] Z. Li, X. Meng, Z. Zhang, Recent development on MoS_2-based photocatalysis: a review, J. Photochem. Photobiol. C: Photochem. Rev. 35 (2018) 39–55.

[9] M.A. Fox, M.T. Dulay, Heterogeneous photocatalysis, Chem. Rev. 93 (1993) 341–357.

[10] A. Fujishima, X. Zhang, D.A. Tryk, TiO_2 photocatalysis and related surface phenomena, Surf. Sci. Rep. 63 (2008) 515–582.

[11] H. Kwon, F.M. Mota, K. Chung, Y.J. Jang, J.K. Hyun, J. Lee, D.H. Kim, Enhancing solar light-driven photocatalytic activity of mesoporous carbon–TiO_2 hybrid films via upconversion coupling, ACS Sustain. Chem. Eng. 6 (2018) 1310–1317.

[12] J. Low, B. Cheng, J. Yu, Surface modification and enhanced photocatalytic CO_2 reduction performance of TiO_2: a review, Appl. Surf. Sci. 392 (2017) 658–686.

[13] F.X. Xiao, S.F. Hung, J. Miao, H.Y. Wang, H. Yang, B. Liu, TiO_2 nanotubes: metal-cluster-decorated TiO_2 nanotube Arrays: a composite heterostructure toward versatile photocatalytic and photoelectrochemical applications, Small 11 (2015) 553.

[14] M. Das, K.G. Bhattacharyya, Oxidation of Rhodamine B in aqueous medium in ambient conditions with raw and acid-activated MnO_2, NiO, ZnO as catalysts, J. Mol. Catal. Chem. 391 (2014) 121–129.

[15] H. Cao, S.L. Suib, Highly efficient heterogeneous photooxidation of 2-propanol to acetone with amorphous manganese oxide catalysts, J. Am. Chem. Soc. 116 (1994) 5334–5342.

[16] M.S. Patil, N. Kitchamsetti, S.R. Mulani, S.R. Rondiya, N.G. Deshpande, R.A. Patil, R.W. Cross, N.Y. Dzade, K.K. Sharma, P.S. Patil, Y.R. Ma, H.K. Cho, R.S. Devan, Photocatalytic behavior of $Ba(Sb/Ta)_2O_6$ perovskite for reduction of organic pollutants: experimental and DFT correlation, J. Taiwan Inst. Chem. Eng. (2021).

[17] M. Singh, B.C. Yadav, A. Ranjan, M. Kaur, S.K. Gupta, Synthesis and characterization of perovskite barium titanate thin film and its application as LPG sensor, Sensor. Actuator. B Chem. 241 (2017) 1170–1178.

[18] N. Kitchamsetti, Y.R. Ma, P.M. Shirage, R.S. Devan, Mesoporous perovskite of interlocked nickel titanate nanoparticles for efficient electrochemical supercapacitor electrode, J. Alloys Compd. 833 (2020) 155134.

[19] N. Kitchamsetti, R.J. Choudhary, D.M. Phase, R.S. Devan, Structural correlation of a nanoparticle-embedded mesoporous $CoTiO_3$ perovskite for an efficient electrochemical supercapacitor, RSC Adv. 10 (2020) 23446–23456.

[20] S. Alkaykh, A. Mbarek, E.E. Ali-Shattle, Photocatalytic degradation of methylene blue dye in aqueous solution by $MnTiO_3$ nanoparticles under sunlight irradiation, Heliyon 6 (2020), e03663.

[21] H. Dai, Y. Zhong, X.Y. Wu, R.X. Hu, L. Wang, Y.C. Zhang, G.K. Fan, X. Hu, J. Li, Z. Yang, Synthesis of perovskite-type $SrTiO_3$ nanoparticles for sensitive electrochemical biosensing applications, J. Electroanal. Chem. 810 (2018) 95–99.

[22] X. Yan, C.L. Zhao, Y.L. Zhou, Z.J. Wu, J.M. Yuan, W.S. Li, Synthesis and characterization of $ZnTiO_3$ with high photocatalytic activity, Trans. Nonferrous Metals Soc. China 25 (2015) 2272–2278.

[23] P.S. Konstas, I. Konstantinou, D. Petrakis, T. Albanis, Development of $SrTiO_3$ photocatalysts with visible light response using amino acids as dopant sources for the degradation of organic pollutants in aqueous systems, Catalysts 8 (2018) 528.

[24] M. Thamima, Y. Andou, S. Karuppuchamy, Microwave assisted synthesis of perovskite structured $BaTiO_3$ nanospheres via peroxo route for photocatalytic applications, Ceram. Int. 43 (2017) 556–563.

[25] N. Pugazhenthiran, K. Kaviyarasan, T. Sivasankar, A. Emeline, D. Bahnemann, R.V. Mangalaraja, S. Anandan, Sonochemical synthesis of porous $NiTiO_3$ nanorods for photocatalytic degradation of ceftiofur sodium, Ultrason. Sonochem. 35 (2017) 342–350.

[26] A. Abedini, S. Khademolhoseini, Cobalt titanate nanoparticles: synthesis, characterization, optical and photocatalytic properties, J. Mater. Sci.: Mater. Electron. 27 (2016) 330–334.

[27] H.Y. He, W.X. Dong, G.H. Zhang, Photodegradation of aqueous methyl orange on $MnTiO_3$ powder at different initial pH, Res. Chem. Intermed. 36 (2010) 995–1001.

[28] N. Kitchamsetti, M.S. Ramteke, S.R. Rondiya, S.R. Mulani, M.S. Patil, R.W. Cross, N.Y. Dzade, R.S. Devan, DFT and experimental investigations on the photocatalytic activities of NiO nanobelts for removal of organic pollutants, J. Alloys Compd. 855 (2021) 157337.

[29] W. Xu, C. Zheng, H. Hua, Q. Yang, L. Chen, Y. Xi, C. Hu, Synthesis and photoelectrochemical properties of $CdWO_4$ and $CdS/CdWO_4$ nanostructures, Appl. Surf. Sci. 327 (2015) 140–148.
[30] R.K. Maurya, S. Bansal, A. Ali, B.H. Reddy, R.S. Singh, Core level XPS study of $MnTiO_3$ using different surface preparation method, AIP Conf. Proc. 2265 (2020), 030380.
[31] N. Kitchamsetti, R.S. Kalubarme, P.R. Chikate, C.J. Park, Y.R. Ma, P.M. Shirage, R.S. Devan, An investigation on the effect of Li-ion cycling on the vertically aligned brookite TiO_2 nanostructure, ChemistrySelect 4 (2019) 6620–6626.
[32] N. Kitchamsetti, P.R. Chikate, R.A. Patil, Y.R. Ma, P.M. Shirage, R.S. Devan, Perforated mesoporous NiO nanostructures for an enhanced pseudocapacitive performance with ultra-high rate capability and high energy density, CrystEngComm 21 (2019) 7130–7140.
[33] S. Kumar, A. Dhiman, P. Sudhagar, V. Krishnan, ZnO-graphene quantum dots heterojunctions for natural sunlight-driven photocatalytic environmental remediation, Appl. Surf. Sci. 447 (2018) 802–815.
[34] W.J. Dong, D.Z. Wang, L.S. Jiang, H. Zhu, H. Huang, J. Li, H. Zhao, C. Li, B. Chen, G. Deng, Synthesis of F doping $MnTiO_3$ nanodiscs and their photocatalytic property under visible light, Mater. Lett. 98 (2013) 265–268.
[35] A. Kubiak, K.S. Ciesielczyk, Z. Bielan, A.Z. Jurek, T. Jesionowski, Synthesis of highly crystalline photocatalysts based on TiO_2 and ZnO for the degradation of organic impurities under visible-light irradiation, Adsorption 25 (2019) 309–325.
[36] N. Li, Y. He, J. Lian, Q. Liu, X. Zhang, X. Zhang, Facile fabrication of a NiO/Ag_3PO_4 Z-scheme photocatalyst with enhanced visible-light-driven photocatalytic activity, New J. Chem. 44 (2020) 12806–12814.
[37] A. Khatri, P.S. Rana, Visible light photocatalysis of methylene blue using cobalt substituted cubic NiO nanoparticles, Bull. Mater. Sci. 42 (2019) 141.
[38] K. Hayat, M.A. Gondal, M.M. Khaled, S. Ahmed, Effect of operational key parameters on photocatalytic degradation of phenol using nano nickel oxide synthesized by sol-gel method, J. Mol. Catal. Chem. 336 (2011) 64–71.